Supporting Information

Enokizono et al. 10.1073/pnas.1222811110

SI Text

Comparison of NMR Spectra of Wild Type and BB-Loop Mutant. To exclude the possibility that the BB-loop mutations disrupt the tertiary structure of the TIR domain, we compared [^{1}H, ^{15}N]-HSQC spectra of both wild-type and TICAM-2 C117H under dilute solution conditions. At 50 μM concentration, the [^{1}H, ^{15}N]-HSQC spectra of the wild type and TICAM-2 C117H (Fig. S1 *A* and *B*) were quite similar, showing that TICAM-2 C117H has a similar structure to the wild type although the signal intensity of the wild type was significantly reduced as a result of oligomerization. The crystal structures of the TIR domains of the wild type and the BB-loop mutant of TLR2 are nearly identical (1), supporting a general model in which the BB-loop mutations do not disrupt the global TIR domain fold. Despite global reduction of the signal intensities in the wild type compared with TICAM-2 C117H, BB-loop residues showed remarkably reduced signal intensity, suggesting that the BB-loop residues are broadened due to dynamic equilibrium between the monomeric and oligomeric states. The exchange broadening effect on Leu122 in the wild type of TICAM-2 TIR and TICAM-2 C117H (Fig. S1 *A* and *B*) was significantly different, consistent with a model in which the homotypic interaction is directly mediated by the BB-loop residues. Although we could not observe NMR spectra of the wild-type TICAM-1 TIR even at dilute concentration, the solubility of TICAM-1 P434H was much improved, and we could obtain a clear NMR spectrum (Fig. S1*C*). After further optimization of the solution condition of the BB-loop mutants, the solubility of TICAM-2 C117H and TICAM-1 P434H was further improved, and the structures of the TIR domains were determined by NMR.

Confirmation of the Yeast Two-Hybrid Experiments by Gel-Filtration Chromatography. In yeast two-hybrid experiments, it is generally difficult to distinguish mutations that disrupt the protein interaction surface from those that disrupt the tertiary structure. To discriminate these two scenarios, the mutant proteins were expressed and subjected to gel-filtration chromatography. Both TICAM-2 C117H and TICAM-2 C117H/E87A/D88A/D89A appeared in the monomer position (Fig. S3 *A* and *B*), but TICAM-2 C117H/E197R/E198R appeared in the void, possibly due to disruption of the tertiary structure (Fig. S3*C*). The NMR structure of TICAM-2 C117H suggests that Glu197 and Glu198 form a salt bridge with Arg95, which raised the possibility that the mutation of Glu197 and Glu198 might destabilize the tertiary structure of the TICAM-2 TIR domain. Therefore, TICAM-2 C117H/R95E was prepared and subjected to gel-filtration chromatography. TICAM-2 C117H/R95E appeared in the void (Fig. S3*D*). Taken together, these results suggest that residues, E87, D88, and D89 of TICAM-2 C117H (designated the "EDD site") interact with Arg522 and Lys523 (the "RK site") on TICAM-1. Gel-filtration chromatography also resulted in TICAM-1 P434H appearing in the monomer position (Fig. S3*E*), consistent with the NMR result (Fig. S1*C*). However, the TICAM-1 P434H/E493R mutant appeared in the void, suggesting that the E493R mutation disrupts the tertiary structure of TICAM-1.

Restrained Docking of Trimeric TICAM-2/TICAM-1 Complex. An optimal model could be identified by considering mutational effects on binding in detail. That is, for each candidate trimer model, a series of mutations were generated *in silico* along with the corresponding changes in binding energy (Table S4). These changes were compared with the yeast two-hybrid assays for each mutant (Tables S2 and S3), and the candidate trimer models were ranked by their agreement with experiment. From such analysis, a narrow cluster consisting of five models (ranks 1, 2, 3, 7, and 8) was defined (Fig. S5).

Reporter Gene Assays of TICAM-1 and TICAM-2 Mutants in Mammalian Cells. TICAM-2-dependent IFN-β promoter activation was studied by the mutation of E87A/D88A/D89A. HEK293FT cells preseeded onto 96-well plates were transfected with empty vector or increasing amounts of expression vector for wild type or mutant TICAM-2 (10, 20, 70 ng per well) together with IFN-β promoter plasmid (25 ng per well) and internal control plasmid (5 ng per well). The total amount of DNA was kept at 100 ng per well by adding empty plasmid. Luciferase activity was measured 24 h after transfection. Next, TICAM-2-TICAM-1–dependent IFN-β promoter activation was studied by the mutation of E87A/D88A/D89A in the similar condition mentioned above with a limiting amount of TICAM-1 expression plasmid (0.1 ng per well). Finally, TICAM-2-TICAM-1–dependent IFN-β promoter activation was studied by the mutation of R522A/K523A in TICAM-1. Cells were transfected with empty vector or expression vector for wild type or mutant TICAM-1 (1 ng per well) and wild-type TICAM-2 (20 ng per well).

All experiments were done in triplicate, and data are shown as means ± SD. Representative data from a minimum of three separate experiments are shown.

Coimmunoprecipitation Assay of TICAM2 and TICAM2 EDD Mutant with TICAM-1. HEK293FT cells preseeded onto six-well plates were transfected with TICAM-1 expression vector (0.2 μg per well), TLR4 and MD2 expression vector (0.2 μg per well), and TICAM-2 expression vector (0.3 μg per well). The total amount of DNA was kept at 2 μg per well by adding empty plasmid. After 24 h from transfection, cells were harvested, and immunoprecipitation assays were performed.

SI Materials and Methods

Protein Expression and Purification. The human TICAM-1 gene encoding the TIR domain (amino acid residues 387–545) with mutation of Pro434 to His was cloned into the pET22b (Novagen) vector with restriction enzymes, NdeI and XhoI (GenBank accession no. NM_182919) and expressed as a His_6-tagged fusion protein at the N terminus. The human TICAM-2 gene encoding the TIR domain (amino acid residues 75–235) with mutation of Cys117 to His was cloned into the pGEX6p-1(GE healthcare) vector with restriction enzymes BamHI and EcoRI (GenBank accession no. NM_021649) and expressed as a GST fusion protein at the N terminus. These vectors were transformed into *Escherichia coli* BL21(DE3) that contains the chaperone expression plasmid pG-Tf2 (Takara). The transformed *E. coli* BL21(DE3) cells were cultured at 37 °C until the OD_{600} reached ~0.6–0.7. The cells were induced with 0.5 mM IPTG and 5 ng/mL tetracycline and then cultured for 18–20 h at 22 °C. The cells were resuspended in lysis buffer [20 mM Tris·HCl (pH7.0), 5 mM DTT, 5 mM EDTA, protease inhibitor mixture (Nacalai) except salts]. TICAM-1 P434H fused with His_6-tag was first purified by Ni^{2+}-NTA affinity chromatography. In contrast, TICAM-2 C117H was purified by Glutathione Sepharose 4B FF affinity chromatography, followed by PreScission protease cleavage. TICAM-1 P434H and TICAM-2 C117H were further purified by size-exclusion chromatography (HiLoad26/60 Superdex-75 pg column; GE Healthcare) in 50 mM Hepes (pH7.0), 10 mM DTT, 75 mM NaCl, and 0.1 mM EDTA.

The pooled fractions of each domain were applied to dialysis and buffer exchange with long-term stabilizing buffer [20 mM AcOH-AcONa (pH 5.0), 10 mM DTT, and 0.1 mM EDTA for TICAM-1 P434H and 40 mM Hepes-NaOH (pH 7.4), 10 mM DTT, 0.1 mM EDTA, and 5% (vol/vol) glycerol for TICAM-2 C117H, respectively].

Finally, each sample solution was concentrated with centricon-3 (MWCO 3 kDa) and exchanged in NMR buffer. NMR Samples were prepared at 0.5 mM TICAM-1 P434H, 20 mM AcOH-AcONa (pH 5.0), 5 mM DTT, 0.1 mM EDTA, 10% D_2O/H_2O, and 0.5 mM TICAM-2 C117H, 40 mM Hepes –NaOH (pH 7.4), 5 mM DTT, 0.1 mM EDTA, 5%(vol/vol) d_{11}-glycerol, 10% D_2O/90% H_2O.

NMR Measurements and Structure Calculation. NMR data for chemical shift assignments for TICAM-1 P434H and TICAM-2 C117H were collected using the suite of triple resonance experiments on Varian UNITY INOVA 600 and 800 spectrometers equipped with a cryogenically cooled probe at 298 K and 293 K, respectively. The data were processed with the NMRPipe software (2) and analyzed using the Sparky3 program (version 3.114) (3). NOE distance restraints were obtained from 3D ^{15}N-NOESY-HSQC (100 ms mixing time) and ^{13}C-NOESY-HSQC spectra (100 ms mixing time). The NMR structures of TICAM-1 P434H and TICAM-2 C117H were determined using the CANDID/CYANA 2.1 (4). Dihedral restraints were derived from backbone chemical shifts using TALOS (5). Chemical shift assignments and NOE and dihedral restraint data have been deposited at BMRB (accession nos. 18882 and 18883 for TICAM-2 and TICAM1, respectively), and the coordinates for the ensemble have been deposited in the Protein Data Bank (PDB ID codes 2mlw and 2mlx for TICAM-2 and TICAM1, respectively).

Yeast Two-Hybrid Analysis. The TIR domains were constructed by direct cloning of two-step PCR products using mutant oligonucleotide primers (6) and subcloned into pGBKT7 and pGADT7 plasmid (Clontech). All mutants were sequenced to confirm the mutation. Yeast two-hybrid assays were conducted in yeast diploid strain, mated with AH109 and Y187, in MATCHMAKER Two-Hybrid System 3 (Clontech).

Liquid cultures were incubated overnight with shaking (220 rpm) at 28 °C and normalized for cell concentration by dilution with synthetic dropout medium (SD medium) such that A_{600nm} = 0.1. After dilution serially, yeast cells were streaked or spotted onto appropriate selection plates and incubated at 28 °C for ~72 h. Interactions between TIR domains of TICAM-1 P434H and TICAM-2 C117H were screened by the observation of yeast growth on media lacking histidine or histidine/adenine. Yeast transformation and screening methods were described in the Yeast Protocols Handbook and the manufacturer's instructions (Clontech).

Restrained Docking Calculations. Two docking methods, HADDOCK (7) and surFit (http://sysimm.ifrec.osaka-u.ac.jp/surFit/), were used to generate representative TICAM-2 TIR homo-dimer models, from which trimeric TICAM-2/TICAM-1 models were then constructed. By ranking the resulting trimeric models by their consistency with the mutagenesis experiments, unfeasible TICAM-2 homodimer models were eliminated. TICAM-1 was then redocked at higher resolution to each of the surviving TICAM-2 homo-dimer models. Final selection was made by carrying out binding energy calculations using the EMPIRE (8) scoring function in combination with structural refinement of the wild-type and mutant forms of the top-scoring trimeric models.

Immunoprecipitation and Immunoblot Analysis. HA-tagged TICAM-1(1–566)-RHIM-mutant (V687A/Q688A/L689A/G690A) and FLAG-tagged TICAM-2(1–235) mutants were subcloned into pEF-BOS vector (9). TLR4 and MD2 expression plasmids were constructed as in a previous report (1). TICAM-1 and TICAM-2 mutants were transfected into HEK293FT cells using Fugene HD. Twenty-four hours after transfection, cells were harvested and lysed by 50 mM Tris·HCl (pH 7.5)-150 mM NaCl-1.0% Nonidet P-40-5 mM Na3VO4-30 mM NaF-X1 Protease inhibitor (Roche). FLAG-tagged TICAM-2 were immunoprecipitated using anti-FLAG mAb (2.5 μg per sample) and Protein G Sepharose (GE healthcare). Total lysates and immunoprecipitated proteins were analyzed by SDS/PAGE and immunoblotting using anti-FLAG pAb (Sigma) and anti-HA mAb (Roche) for the detection of TICAM-2 and TICAM-1.

Luciferase Reporter Gene Assay. Mutants of TICAM-1(1–566) and TICAM-2(1–235) were generated using PCR and subcloned into pEF-BOS vector. HEK293FT cells (Invitrogen) were maintained in Dulbecco's Modified Eagle's medium high glucose supplemented with MEM NEAA (Gibco), 10% heat-inactivated FCS, and antibiotics. Cells were transfected with TICAM-1 and TICAM-2 expression plasmids, IFN-β promoter plasmid, and an internal control plasmid coding *Renilla* luciferase using Fugene HD (Promega). Twenty-four hours after transfection, cells were lysed with Reporter Lysis Buffer (Promega). Luciferase activity was measured using Dual-Glo Luciferase Assay System (Promega). The *Firefly* luciferase activity was normalized to the *Renilla* activity and expressed as the fold-stimulation relative to the activity of vector-transfected cells. All assays were performed in triplicate.

1. Tao X, Xu Y, Zheng Y, Beg AA, Tong L (2002) An extensively associated dimer in the structure of the C713S mutant of the TIR domain of human TLR2. *Biochem Biophys Res Commun* 299(2):216–221.
2. Delaglio F, et al. (1995) NMRPipe: A multidimensional spectral processing system based on UNIX pipes. *J Biomol NMR* 6(3):277–293.
3. Goddard TD, Kneller DG (2004) SPARKY 3 (University of California, San Francisco).
4. Güntert P (2004) Automated NMR structure calculation with CYANA. *Methods Mol Biol* 278:353–378.
5. Cornilescu G, Delaglio F, Bax A (1999) Protein backbone angle restraints from searching a database for chemical shift and sequence homology. *J Biomol NMR* 13(3):289–302.
6. Landt O, Grunert HP, Hahn U (1990) A general method for rapid site-directed mutagenesis using the polymerase chain reaction. *Gene* 96(1):125–128.
7. de Vries SJ, van Dijk M, Bonvin AM (2010) The HADDOCK web server for data-driven biomolecular docking. *Nat Protoc* 5(5):883–897.
8. Liang S, Zheng D, Zhang C, Standley DM (2011) Fast and accurate prediction of protein side-chain conformations. *Bioinformatics* 27(20):2913–2914.
9. Mizushima S, Nagata S (1990) pEF-BOS, a powerful mammalian expression vector. *Nucleic Acids Res* 18(17):5322.

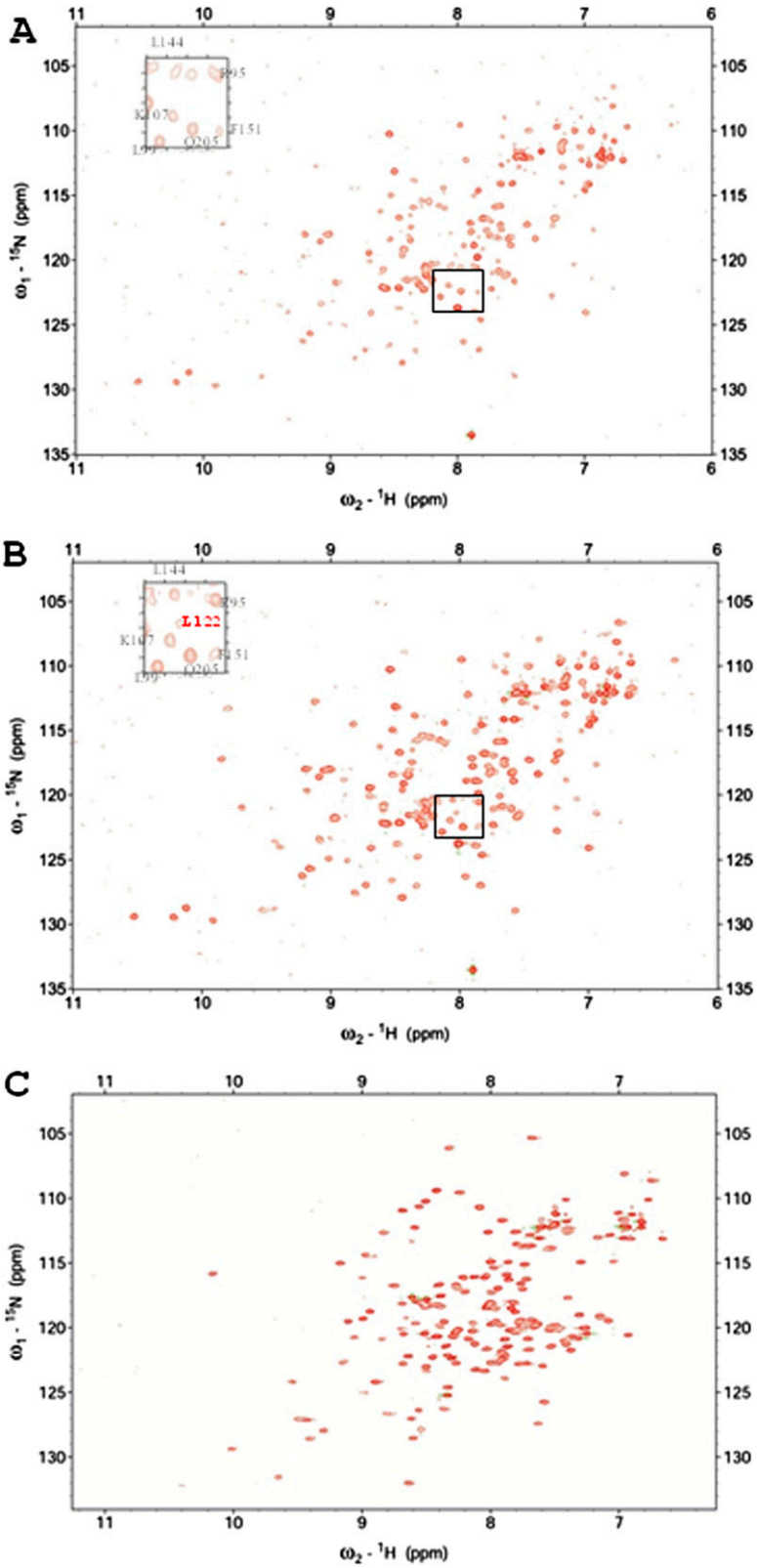

Fig. S1. [^{1}H,^{15}N]-HSQC spectra of the TIR domains of TICAM-1 and TICAM-2. (*A* and *B*) Comparison of HSQC spectra of the TICAM-2 wild type and C117H mutant under the same buffer conditions [50 μM ^{15}N-labeled proteins, 40 mM Hepes-NaOH (pH 7.2), 10 mM DTT, 10% glycerol, 90% H_2O/10% D_2O at 20 °C]. The *Inset* focused on Leu122 in the BB-loop in the wild type (*A*) and C117H mutant (*B*). (*C*) HSQC spectra of TICAM-1 P434H under acidic buffer conditions [0.3 mM ^{15}N-labeled protein, 20 mM AcOH buffer (pH 5.0), 10 mM DTT, 0.1 mM EDTA, 90% H_2O/10% D_2O at 20 °C].

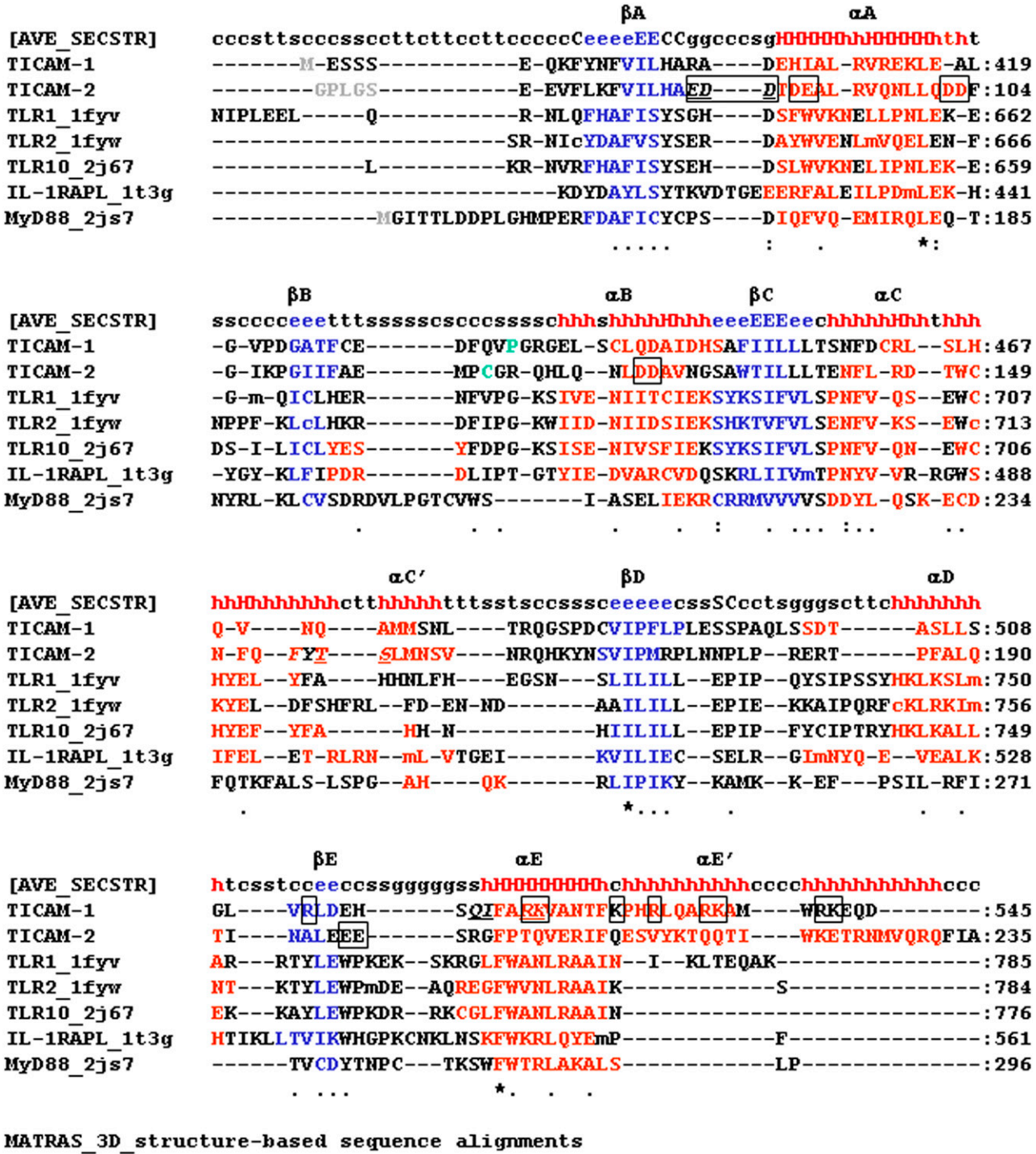

Fig. S2. Structure-based sequence alignments of TIR-domains. Structure-based sequence alignments were generated by the MATRAS web server. The average secondary structural elements of the TICAM-1 TIR are labeled on the top. α-Helices and β-strands are shown in red and blue, respectively. The boxes indicate acidic residues specific to the TICAM-2 TIR domain and basic residues specific to TICAM-1 TIR domain. Italics show interaction sites.

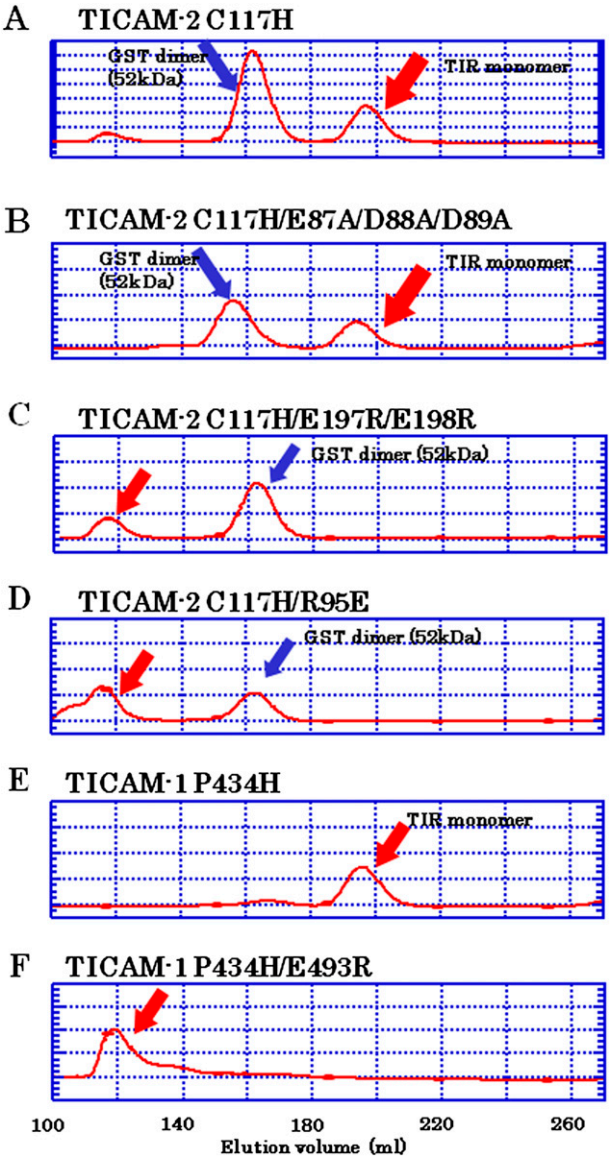

Fig. S3. Gel-filtration analysis of TIR domain mutants of TICAM-1 and TICAM-2. (*A*) TICAM-2 C117H, (*B*) TICAM-2 C117H/E87A/D88A/D89A, (*C*) TICAM-2 C117H/E197R/E198R, (*D*) TICAM-2 C117H/R95E, (*E*) TICAM-1 P434H, and (*F*) TICAM-1 P434H/E493R. The TIR monomer in *A*, *B*, and *E* indicates that elution volume is compatible with monomer size (~18 kDa). In *C*, *D*, and *F*, gel-filtration chromatography peaks appeared in the void position due to formation of high-molecular weight soluble aggregates.

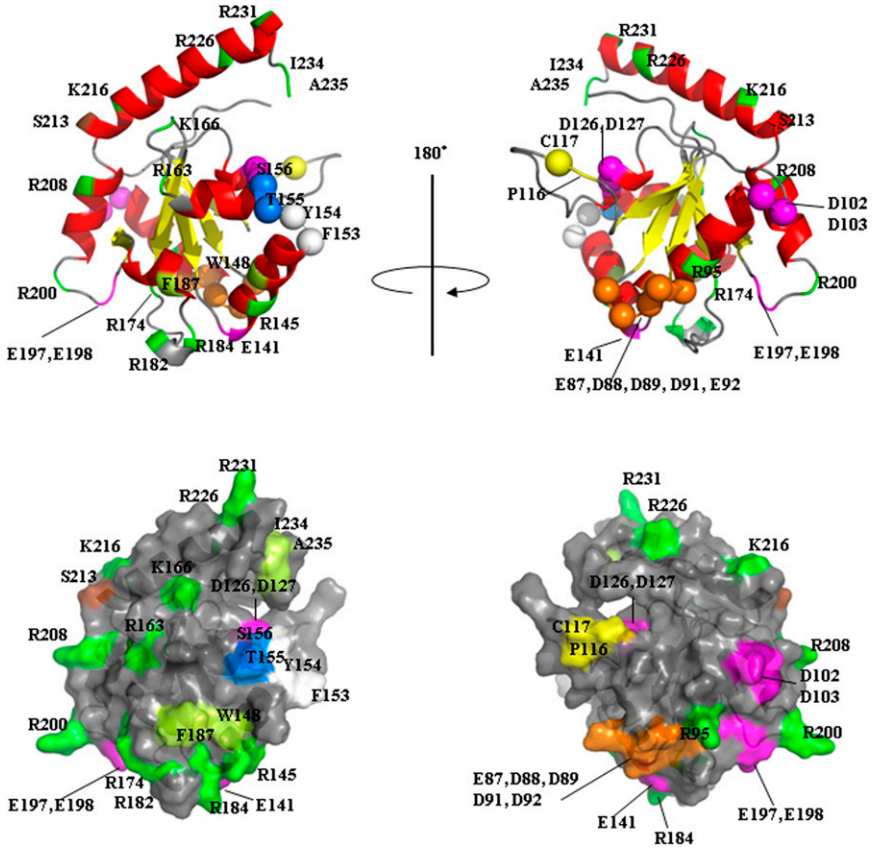

Fig. S4. Summary of mutations of TICMA-2 TIR applied to yeast two-hybrid assays. All mutations applied to yeast two-hybrid assays were mapped on the TIR domain of TICAM-2 C117H. Selected mutations are located on the exposed surface of the α-helices and the loop regions. Acidic residues are shown in orange and magenta. Basic residues are shown in green. Hydrophobic residues are shown in yellow-green. Pro116 and Cys117 are shown in yellow. Thr155 and Ser156 are shown in blue. Phe153 and Tyr154 are shown in white.

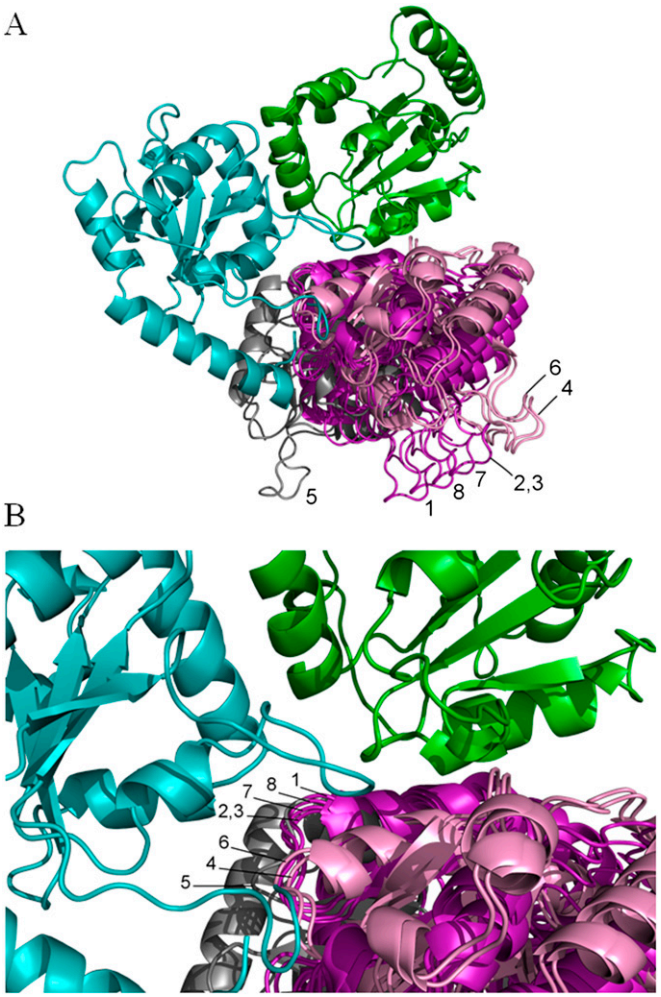

Fig. S5. Ensemble of top-ranked trimer models. (*A*) A global view of the top eight models is shown. (*B*) A close-up view of the top-ranked models at the TICAM-1/TICAM-2 interface is shown.

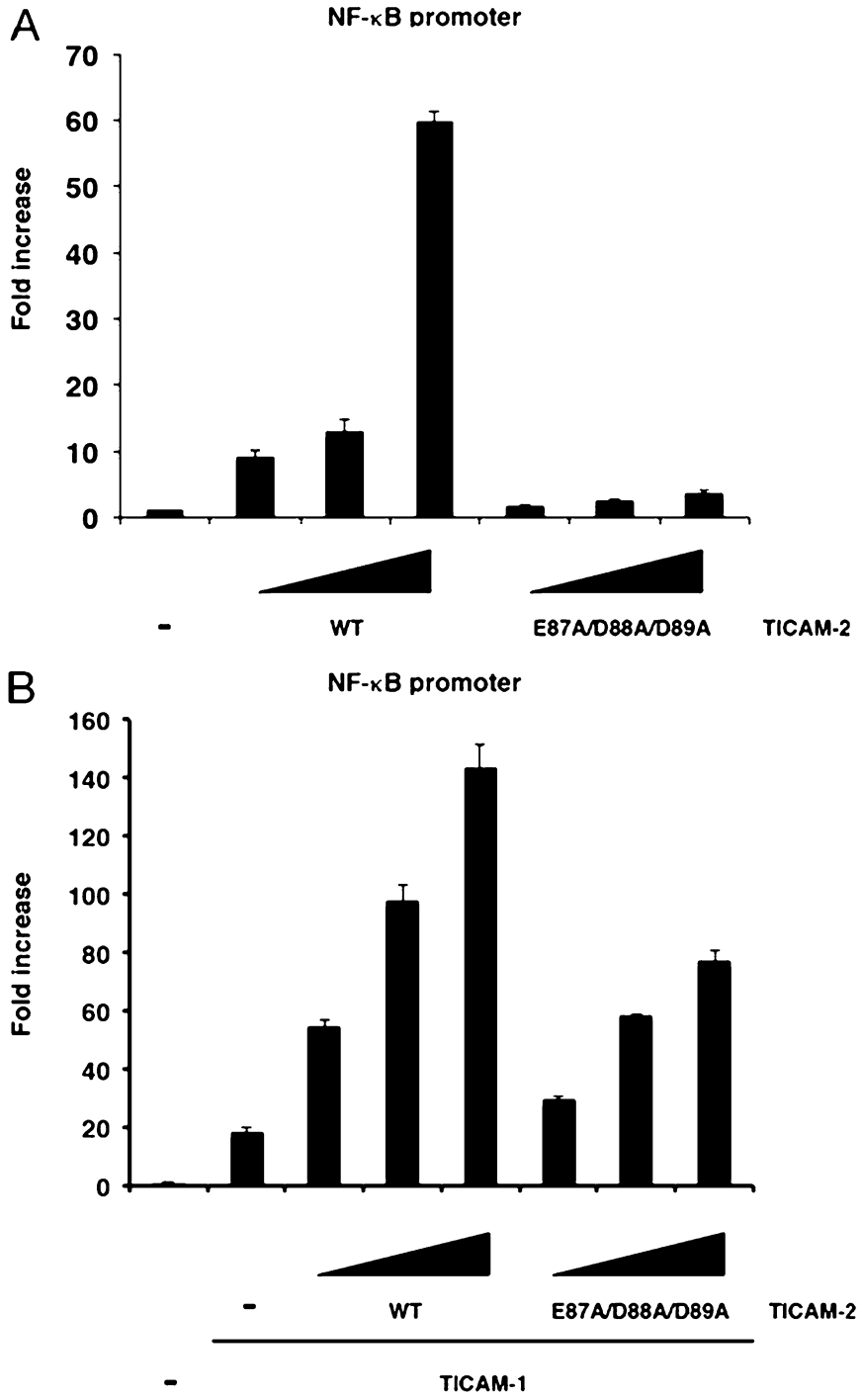

Fig. S6. Reporter assays of NF-κB activation. (*A*) HEK293FT cells preseeded onto 96-well plates were transfected with empty vector or increasing amounts of expression vector for wild-type or mutant TICAM-2 (10, 20, 70 ng per well) together with NF-κB reporter plasmid (25 ng per well) and internal control plasmid (5 ng per well). The total amount of DNA was kept at 100 ng per well by adding empty plasmid. Luciferase activity was measured 24 h after transfection. (*B*) TICAM-2-TICAM-1–dependent NF-κB activation. Cells were transfected with empty vector or indicated TICAM-2 expression plasmids (10, 20, 70 ng per well) together with a limiting amount of TICAM-1 expression plasmid (0.1 ng per well), NF-κB reporter plasmid (25 ng per well), and internal control plasmid (5 ng per well). Representative data from a minimum of three separate experiments are shown.

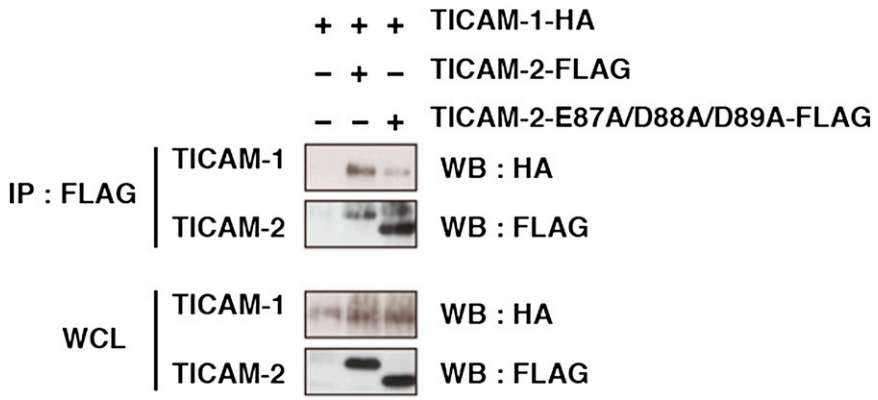

Fig. S7. Immunoprecipitation and immunoblot analysis of TICAM-1 and TICAM-2 interaction.

Table S1. Structural statistics for the 20 structures of lowest energy

	TICAM-1	TICAM-2
NOE distance restraints		
All	3,254	2,699
Sequential ($\|i - j\| = 1$)	1,954	1,481
Medium range ($2 \leq \|i - j\| \leq 4$)	640	529
Long range ($\|i - j\| > 4$)	660	689
Dihedral angle restraints (derived from TALOS)		
φ	104	128
ψ	104	135
Violations		
Distance > 0.5 Å	0	0
Angle > 5°	0	0
rmsd from the mean coordinates (secondary structures)*		
Backbone heavy atoms, Å	0.45	0.50
All heavy atoms, Å	0.84	1.01
Ramachandran plot statics, %†		
Residues in most favorable regions, %	71.6	77.7
Residues in additional allowed regions, %	27.7	22.0
Residues in generously allowed regions, %	0.7	0.3
Residues in disallowed regions, %	0.0	0.0

*The rmsd were calculated for the core region (395–427,442–527) of TICAM-1, and region (83–110,150–215) of TICAM-2.
†Values were calculated with PROCHEK.

Table S2. Summary of results of yeast two-hybrid analyses for mutation of TICAM-1

		Interaction (yeast growth)	
Number of amino acid	Secondary structure	Homotypic	Heterotypic
TICAM-1 (E387-D545)		TICAM-1	TICAM-2
P434H	BB-loop	–	+
R512A	DD-loop	+	+
R522A	αE-helix	+	–
K523A	αE-helix	+	–
R522A/K523	αE-helix	+	–
K529A	αE-helix	+	+
K529A/R532A	αE,αE′-helix	+	+
R532A	αE′-helix	+	+
R541A/K542A	αE′-helix	+	+
P434H/R512A		–	+
P434H/R522A/K523A		–	–
P434H/K529A		–	+
P434H/R532A		–	+
D484A	CD-loop	+	+
E493A	DD-loop	–	–
P434H/D484A		–	+
S495R/A497R	DD-loop	+	+
S495R/A497R/Q498R		+	+
E493R/S495R/A497E/Q498R	DD-loop	–	–
P496G	DD-loop	+	+

+, indicates that yeast can grow on SD-LWHA medium; –, indicates that yeast cannot grow on SD-LWHA medium. Empty cells indicate no data.

Table S3. Summary of results of yeast two-hybrid analyses for mutation of TICAM-2

		Interaction (yeast growth)	
Number of amino acid	Secondary structure	Homotypic	Heterotypic
TICAM-2 (E75-A235)		TICAM-2	TICAM-1
P116H	BB-loop	–	–
C117H	BB-loop	–	–
E87A/D88A/D89A	AA-loop		–
D91A/E92A	αA-helix		+
D102A/D103A	AB-loop		+
D126A/D127A	αB-helix		+
E197A/E198A	EE-loop		–
S64-A235	Extension of N terminus	+	+
E70-A235	Extension of N terminus	+	+
R95A	αA-helix	–	–
E141R	CC-loop	+	+
R231E	C terminus	+	+
R95A/R231E		–	–
E141R/R231E		+	+
R95A/E141R/R231E		–	–
E75-S213*	deletion of C terminus	–	–
E75-R226*	deletion of C terminus	+	+
I234E/A235D	C terminus	+	+
R231E/I234E/A235D	C terminus	+	+
C117H/E114R	BB-loop	–	
C117H/R119E	BB-loop	–	
C117H/E114R/R119E	BB-loop	–	

+, indicates that yeast can grow on SD-LWHA medium; –, indicates that yeast cannot grow on SD-LWHA medium. Empty cells indicate no data.

Table S4. *In silico* binding energy calculations for trimeric models ranked 1–5

	Rank				
Type of amino acid	1	2	3	4	5
TICAM-1 (E387-D545)					
P434H	+	+	+	+	+
R512A	+	+	+	–	+
R522A	–	–	–	–	–
K523A	–	–	–	–	–
R522A/K523	–	–	–	–	–
K529A	+	+	+	+	+
K529A/R532A	+	+	+	+	+
R532A	+	+	+	+	+
R541A/K542A	+	+	+	+	+
P434H/R512A	+	+	+	+	+
P434H/R522A/K523A	–	–	–	–	–
P434H/K529A	+	+	+	+	+
P434H/R532A	+	+	+	+	+
D484A	+	+	+	+	+
E493A	+	+	+	–	+
P434H/D484A	+	+	+	+	+
S495R/A497R	+	+	+	+	+
S495R/A497R/Q498R	+	+	+	+	+
E493R/S495R/A497E/Q498R	+	+	+	+	+
P496G	+	+	+	+	+
P434H/Q518A/I519A	–	–	–	–	–
TICAM-2 E75-A235)					
P116H	+	+	+	+	+
C117H	+	+	+	–	+
E87A/D88A/D89A	–	–	–	–	–
D91A/E92A	–	–	+	+	–
D102A/D103A	+	+	+	+	+
D126A/D127A	+	+	+	+	+
E197A/E198A	+	–	–	+	+
R95A	+	+	+	+	+
E141R	+	+	+	–	+
R231E	+	+	+	+	+
R95A/R231E	+	+	+	+	+
E141R/R231E	+	+	+	–	+
R95A/E141R/R231E	+	+	+	+	+
I234E/A235D	+	+	+	+	+
R231E/I234E/A235D	+	+	+	+	+
F153A/Y154S	+	–	–	–	+
T155A/S156A	–	–	–	–	–

A gray background indicates disagreement between calculation and experiment.